THE JOURNAL OF PHYSICAL CHEMISTRY B

Article

pubs.acs.org/JPCB

# Bridging Hydroxyls on Anatase $TiO_2$(101) by Water Dissociation in Oxygen Vacancies

Immad M. Nadeem,[†,‡] George T. Harrison,[†] Axel Wilson,[†] Chi L. Pang,[†] Jörg Zegenhagen,[‡] and Geoff Thornton*[,†]

[†]London Centre for Nanotechnology and Department of Chemistry, University College London, 20 Gordon Street, London, WC1H 0AJ, U.K.

[‡]Diamond Light Source Ltd., Harwell Science and Innovation Campus, Didcot, Oxfordshire, OX11 0DE, U.K.

**ABSTRACT:** Titanium dioxide is a promising candidate for photocatalytic $H_2$ fuel production, and understanding water splitting on $TiO_2$ surfaces is vital toward explaining and improving the generation of $H_2$. In this work, we electron irradiate anatase $TiO_2$(101) at room temperature to create metastable surface oxygen vacancies in order to investigate their ability to dissociate $H_2O$. Our scanning tunneling microscopy investigations suggest that the surface oxygen vacancies can dissociate $H_2O$ by forming bridging OH species. This claim is supported by theoretical calculations from the literature and our previously published spectroscopic measurements.

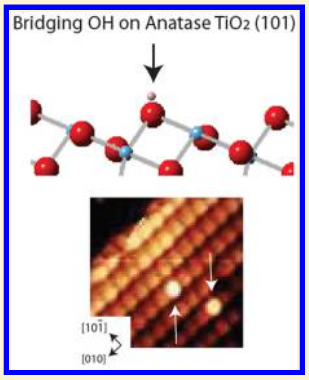

## 1. INTRODUCTION

Light harvesting metal oxides photocatalytically split water to produce $H_2$ fuel.[1] Since Honda and Fujishima[2] showed the potential of $TiO_2$ in this respect, it has been widely studied.[3−6] $TiO_2$ is a low cost, highly photostable, and nontoxic material that displays high catalytic efficiency.[7] Three polymorphs of $TiO_2$ exist in nature: rutile, anatase, and brookite.[8] Anatase and rutile are the most active and studied polymorphs with research extending from engineering materials[3−6] to fundamental work.[9−13] *Rutile $TiO_2$(110)* ($R_{110}$) and *anatase $TiO_2$(101)* ($A_{101}$) are the most stable faces of the respective polymorphs. The former has been the focus of numerous publications,[9−11] whereas research on the latter is less well documented.

$A_{101}$ consists of 5 ($Ti_{5c}$) and 6 ($Ti_{6c}$) coordinate Ti and 2 ($O_{2c}$) and 3 ($O_{3c}$) coordinate O in a sawtooth-like geometry[14,15] (see Figure 1). In principle, the surface can maintain *bridging OH* ($OH_{br}$) (i.e., H adatom on $O_{2c}$) and *terminal OH* ($OH_t$) (i.e., OH adsorbed to $Ti_{5c}$). Scanning tunneling microscopy (STM) images of $A_{101}$ show trapezoidal terraces and sphere-like features that represent a $Ti_{5c}$−$O_{2c}$ pair[14] (see Figure 2). Electron irradiation of $A_{101}$ creates *surface $O_{2c}$ vacancies* ($V_o$) that are unstable above 200 K and migrate to the subsurface and bulk.[16−18]

The temperature and pressure dependence of $H_2O$ adsorption on $A_{101}$ has been examined.[18−23] In ultrahigh vacuum (UHV), there is little or no evidence of $H_2O$ adsorption at room temperature, although adsorption is increasingly favored below 298 K.[20] In UHV at 6 K, STM tip pulsing (a voltage pulse applied to the surface via the STM tip) can transform $H_2O$ into features thought to be $OH_t$.[22] Co-dosing $O_2$ and $H_2O$ on $A_{101}$ at 105 K and subsequently annealing for 10 min at room temperature, followed by STM (at 6 K), also yields features thought to be $OH_t$.[18] In UHV at 120 K, water has been adsorbed on $A_{101}$ with photoemission measurements collected at intervals from 160 to 400 K. The results indicate that water adsorbs in a mixed associative and dissociative state below 300 K.[21] At room temperature, photoemission measurements of $A_{101}$ under exposure to water pressures of 0.6−6 mbar indicate mixed associative and dissociative adsorption of water.[23] In UHV, at 100 K and under UV illumination, $H_2O$ adsorbed on $A_{101}$ has been observed to generate gaseous OH species. This has been interpreted as the adsorbed $H_2O$ dissociating into $OH_{br}$ and $OH_t$ where the latter leaves the surface.[24] As for theory, first-principles molecular dynamics calculations predict that $H_2O$ can dissociate in $V_o$[25,26] and that the $A_{101}$ and liquid water interface (at 300−400 K) can maintain $OH_t$ and $OH_{br}$ species.[27,28]

In the literature, scanning probe microscopy (SPM) of $OH_t$[18,22] on $A_{101}$ is reported, while SPM of $OH_{br}$[29] is relatively briefly discussed. Similar to $A_{101}$, $R_{110}$ consists of $Ti_{5c}$, $Ti_{6c}$, $O_{2c}$, and $O_{3c}$ species, with the two surfaces differing in their bond angles.[9−11] $OH_{br}$ can form on $R_{110}$ via dissociation of $H_2O$ from the residual vacuum at $V_o$ sites.[9,10] In previous work,[30] we presented spectroscopic evidence of OH formation on the $A_{101}$ surface via $H_2O$ dissociation in $V_o$. In this paper, we describe an STM study that identifies the OH species as $OH_{br}$.

**Special Issue:** Miquel B. Salmeron Festschrift

**Received:** July 14, 2017
**Revised:** September 12, 2017
**Published:** October 9, 2017

DOI: 10.1021/acs.jpcb.7b06955
*J. Phys. Chem. B* 2018, 122, 834−839

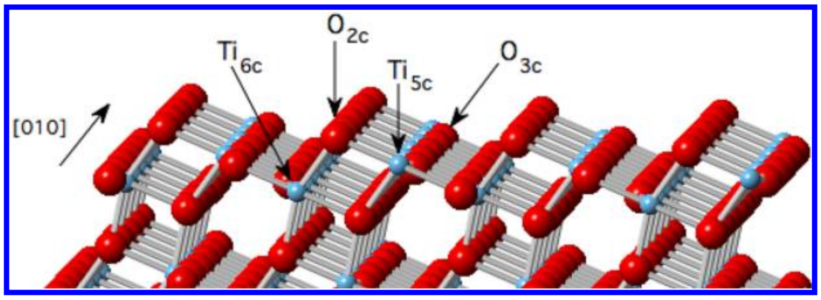

**Figure 1.** Illustration of the $A_{101}$ surface with the $Ti_{5c}$, $Ti_{6c}$, $O_{3c}$, and $O_{2c}$ labeled.

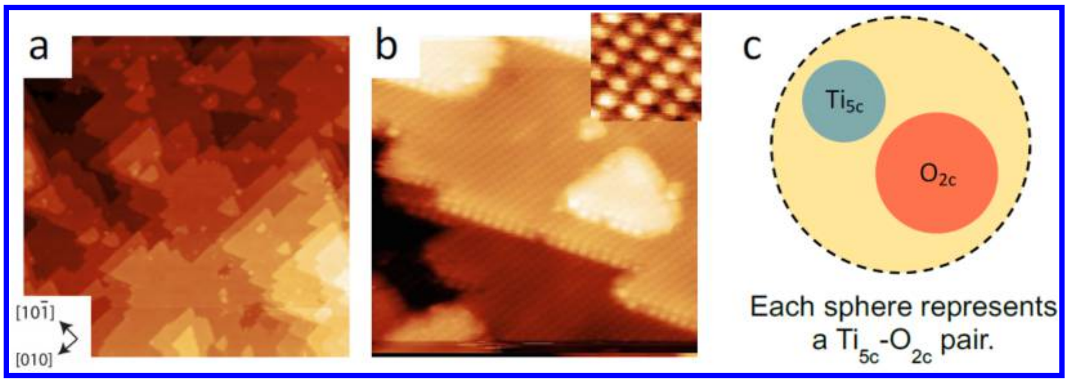

**Figure 2.** (a) 100 × 100 $nm^2$ STM image of $A_{101}$ ($V_s = +1.6$ V, $I_t = 0.4$ nA). (b) 15 × 15 $nm^2$ STM image of $A_{101}$ ($V_s = +1.1$ V, $I_t = 0.6$ nA) with the inset (2 × 2 $nm^2$) illustrating the sphere-like features observed with STM. (c) Illustration that each sphere-like feature in STM represents a $Ti_{5c}$–$O_{2c}$ pair.

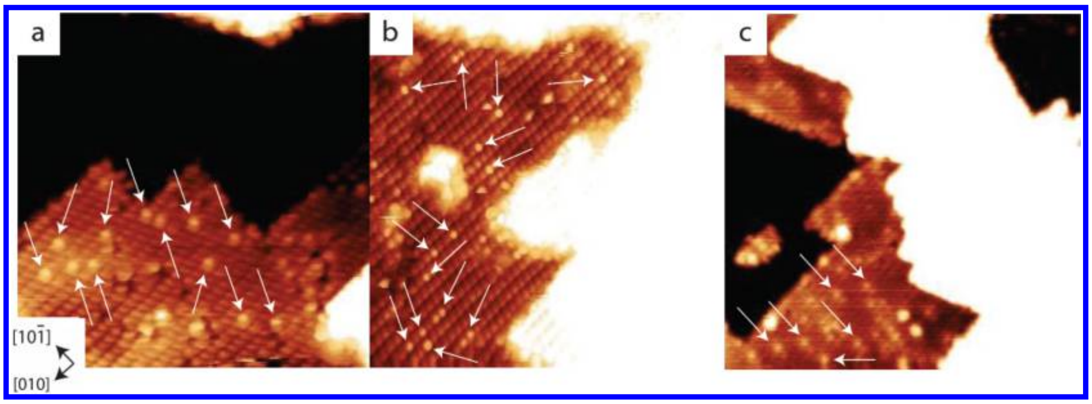

**Figure 3.** (a) 13 × 13 $nm^2$ STM image ($V_s = +1.6$ V, $I_t = 0.5$ nA) of $A_{101}$ after electron irradiation at 500 eV, for 30 s and at a density of 37 $\mu A.cm^{-2}$. (b) 15 × 15 $nm^2$ STM image ($V_s = +1.03$ V, $I_t = 0.3$ nA) of $A_{101}$ after electron irradiation at 500 eV, for 60 s and at a density of 37 $\mu A.cm^{-2}$. (c) 23 × 23 $nm^2$ STM image ($V_s = +1.5$ V, $I_t = 0.4$ nA) of $A_{101}$ after electron irradiation at 50 eV, for 30 s and at a density of 74 $\mu A.cm^{-2}$.

## 2. EXPERIMENTAL SECTION

A natural $A_{101}$ single crystal (3 × 3 × 1 $mm^3$) was purchased from *Pi Kem* and was mounted onto a Ta plate with Ta strips. The sample was prepared in UHV with cycles of $Ar^+$ sputtering ($P_{Ar} = 5 \times 10^{-5}$ mbar, 1 kV, 10 $\mu A.cm^{-2}$, 20 min) and annealing ($T < 1023$ K, 10 min).[31] Low energy electron diffraction (LEED) and Auger electron spectroscopy (AES) were used to ensure an ordered and contaminant free surface (below the detection limits of AES) for STM measurements. The STM used is an *Omicron* UHV AFM/STM instrument operated in constant current mode at room temperature using electrochemically etched tungsten tips, which were degassed in UHV and conditioned during scanning with voltage pulses of up to 10 V. All STM imaging was carried out by tunneling into empty states using positive sample bias voltages in the range from 1 to 1.6 V. The base pressure of the instrument was $5 \times 10^{-10}$ mbar.

An outgassed filament was used for electron irradiation, with a negative bias with respect to the grounded sample. The front face of the sample was approximately 2 cm from the filament, and the drain current from the sample was used to monitor the electron flux. During irradiation, the UHV chamber pressure increased up to the low $10^{-8}$ mbar range with a $H_2O$ partial pressure up to the low $10^{-9}$ mbar region. Immediately after irradiation, the pressure returned to the $10^{-10}$ mbar region. The irradiation stimulated chamber pressure rise is largely attributed to residual UHV gases—$H_2$, $H_2O$, CO, and $CO_2$. At room temperature, $H_2O$ has been experimentally shown to react with $V_o$ to form an $OH_{br}$ defect site on $A_{101}$[30] and $R_{110}$.[9,10] However, at room temperature, there is no evidence to suggest that either CO or $CO_2$ react with $V_o$ on $A_{101}$[30] or $R_{110}$.[9,10] Therefore, the effect of $H_2O$ on $V_o$ can be investigated in the presence of CO and $CO_2$. During irradiation, the sample is expected to be

DOI: 10.1021/acs.jpcb.7b06955
J. Phys. Chem. B 2018, 122, 834−839

mildly heated by electrons emitted from the filament. It takes at least 15 min to transfer the sample from the electron irradiation position to the STM and achieve tunneling conditions. STM presented little or no thermal drift, suggesting that the sample had returned to or was very close to room temperature. This indicates a mild increase in temperature during electron irradiation. The reactivity of the $V_o$ created by electron-irradiation with residual $H_2O$ in UHV (i.e., at the base pressure and during electron irradiation) was investigated with STM. We define a monolayer (ML) as corresponding to the number of surface $Ti_{5c}$—$O_{2c}$ pairs (density: 5.17 $nm^{-2}$). ML coverages are given as averaged values ± two standard deviations.

## 3. RESULTS AND DISCUSSION

Figure 3 shows the $A_{101}$ surface after three electron irradiation events. Images of the electron irradiated surface contain a number of bright features (marked with white arrows in Figure 3) that we identify as $OH_{br}$ groups formed via $H_2O$ dissociation in $V_o$. The density of bright features in Figure 3 is reported in Table 1 and is approximately 0.05 ML, independent of the electron irradiation conditions. Theory and experiment suggest that $A_{101}$ surface defects act as excess electron "traps", where the excess electrons are loosely bound to the defect.[27,30,32] In particular, $OH_{br}$ species on $A_{101}$ are predicted to maintain trapped charge at the $Ti_{5c}$ site adjacent to the $OH_{br}$.[27] Our previously published two-photon photoelectron (2PPE) spectroscopy and UV photoelectron spectroscopy (UPS) work[30] shows that electron irradiated $A_{101}$ can maintain excess electrons beyond thermally equilibrated levels on the surface as OH species. While these earlier results indirectly support the electron irradiation induced formation of $OH_{br}$ (via $H_2O$ reacting with the $V_o$), STM allows us to image the position of the OH species. A high-resolution image of part of the surface imaged in Figure 3b is shown in Figure 4. The positioning of the bright feature is above the sphere-like feature of the as-prepared surface. This is consistent with the formation of $OH_{br}$ with H bound to the $O_{2c}$. On $A_{101}$, $OH_t$[18,22] appear as dimer-like features. Additionally, the appearance of the bright features is reminiscent of $OH_{br}$ observed on $R_{110}$.[9,10] This suggests that the bright features are surface $OH_{br}$ on $A_{101}$ formed via the dissociation of $H_2O$ in a $V_o$.

**Table 1. Surface ML Coverages of the Electron Irradiated $A_{101}$ Presented in Figure 3**

| electron energy (eV) | current density ($\mu$A.cm$^{-2}$) | duration (s) | ML coverage |
|---|---|---|---|
| 500 | 37 | 30 | 0.05 ± 0.01 |
| 500 | 37 | 60 | 0.05 ± 0.01 |
| 50 | 74 | 30 | 0.04 ± 0.01 |

Theory predicts that $H_2O$ dissociation in $V_o$ on $A_{101}$ forms a pair of adjacent $OH_{br}$.[25,26] On $R_{110}$, this type of behavior is observed experimentally, with $OH_{br}$ forming in adjacent pairs.[9,10] The $OH_{br}$ subsequently diffuse (i.e., H adatom diffusion) in the [001] and [1$\bar{1}$0] direction through thermally activated pathways, where diffusion in the latter direction can be promoted by $H_2O$.[33,34] Our STM results for $A_{101}$ show that the OH related bright features are largely immobile on the surface. Hence, the bright features should exist as adjacent pairs representing two $OH_{br}$. In contrast, the data in Figure 3 show that the bright features are well dispersed. This discrepancy could arise from thermally activated $OH_{br}$ migration caused by heating from the filament during electron irradiation or could be due to $H_2O$ induced mobility when the $H_2O$ partial pressure increases during electron irradiation.[33,34] An alternative perspective could be that the bright features are not paired as, during electron irradiation, $OH_{br}$ are being formed and desorbed simultaneously—as is the case on $R_{110}$.[35] Additionally, there may be a complex series of steps where paired $OH_{br}$ initially move quickly away from each other and subsequently over time this movement could slow down and stop after the species are spread over the surface in the most energetically favorable distribution.

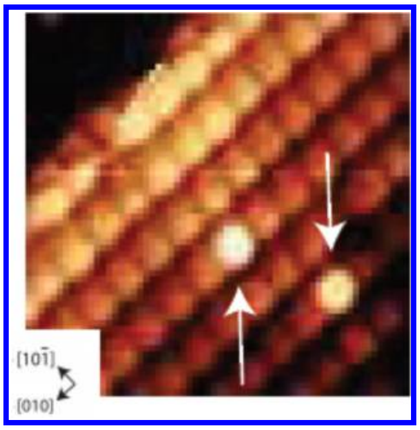

**Figure 4.** 3.5 × 3.5 $nm^2$ STM image ($V_s$ = +1.2 V, $I_t$ = 0.4 nA) of the $A_{101}$ surface after electron irradiation conditions given for Figure 3b. STM image showing that the bright feature exists above the sphere-like feature on $A_{101}$ where each sphere-like feature represents a surface $Ti_{5c}$—$O_{2c}$ pair.

On $R_{110}$, the H adatom (associated with $OH_{br}$ species) can be removed (pulsed off) with approximately +3 V STM tip pulses.[9,10,36] On $A_{101}$, STM tip pulsing (in the range +2.7 to +3.5 V) has been reported to convert $OH_t$ to $O_2$.[18,22] However, the bright features under discussion do not pulse off or convert with +3 to +4 V pulses, suggesting that $OH_{br}$ species on $A_{101}$ are energetically more stable than those on $R_{110}$. This could result in less mobility and greater resistance to STM tip pulsing. Although $R_{110}$ and $A_{101}$ can maintain defects/adsorbates at similar sites, the behavior of these species has been shown to be different; e.g., at room temperature, $V_o$ can exist on the $R_{110}$ surface, whereas, on $A_{101}$, $V_o$ migrates toward the bulk.[16,36] Hence, it is reasonable to suggest that other defects (such as $OH_{br}$) also exhibit different characteristics. Therefore, on $R_{110}$, pulsing can remove $OH_{br}$, whereas this would not necessarily be the case with $A_{101}$. STM tip pulsing beyond +4 V resulted in a "tip-change" which prevented high-resolution, atomically resolved STM images from being recorded.

To further probe the origin of the bright features created by electron irradiation, the surface imaged in Figure 3a was subjected to progressive electron irradiation without surface repreparation (see Figure 5 and Table 2). Each successive electron irradiation condition consists of an increase in the density of electrons irradiating the surface, whereas the electron energy and duration of irradiation were fixed at 500 eV and 30 s, respectively. As is shown in Table 2, this resulted in an increase in bright feature density as the electron density was increased. This likely arises from an increase in the density of electrons irradiating the surface that would increase the number of $V_o$ being created and subsequently result in more $H_2O$ molecules quenching them to form $OH_{br}$. Another point of

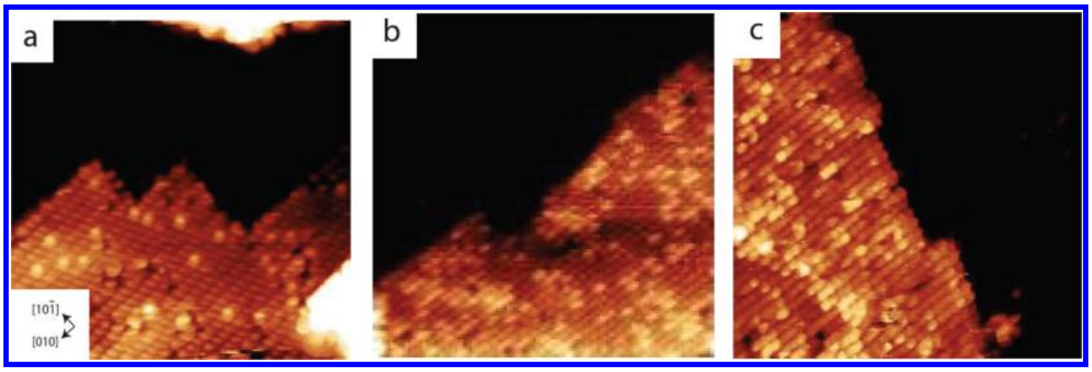

**Figure 5.** STM images obtained after $A_{101}$ has been progressively electron irradiated (without surface repreparation). (a) 13 × 13 nm$^2$ STM image ($V_s$ = +1.6 V, $I_t$ = 0.5 nA) of $A_{101}$ after electron irradiation at 500 eV, for 30 s and at a density of 37 $\mu$A.cm$^{-2}$. This image is identical to Figure 3a. (b) 15 × 15 nm$^2$ STM image ($V_s$ = +1.6 V, $I_t$ = 0.4 nA) after the surface in part a was electron irradiated at 500 eV, for 30 s and at a density of 74 $\mu$A.cm$^{-2}$. (c) 15 × 15 nm$^2$ STM image ($V_s$ = +1.0 V, $I_t$ = 0.3 nA) after the surface in part b was electron irradiated at 500 eV, for 30 s and at a density of 150 $\mu$A.cm$^{-2}$.

**Table 2. Surface ML Coverages of the Electron Irradiated $A_{101}$ Presented in Figure 5**

| electron energy (eV) | current density ($\mu$A cm$^{-2}$) | duration (s) | ML coverage |
|---|---|---|---|
| 500 | 37 | 30 | 0.05 ± 0.01 |
| 500 | 74 | 30 | 0.20 ± 0.06 |
| 500 | 150 | 30 | 0.22 ± 0.08 |

interest—see Figure 5b and c—is that the bright features appear to begin to cluster. This clustering phenomenon may be associated with $OH_{br}$ stabilization at higher coverages. $V_o$ have been reported to form subsurface vacancy clusters,[16] presumably due to favorable energetics and stabilization.

Let us now consider other possible origins of the bright features observed in Figures 3−5. Post-electron irradiation, we do not expect to observe $V_o$ on $A_{101}$. In our experiment, we operate at room temperature where the sample is heated by the filament during electron irradiation followed by at least 15 min required to transfer the sample from the electron irradiation position to tunneling conditions for STM. Subsequently, a further duration of time is necessary to obtain high resolution "atomic-resolved" STM images. Given that $V_o$ start to move toward the bulk at temperatures as low as 200 K,[16] little or no $V_o$ will exist on the surface with our experimental procedure. STM at 78 K of electron irradiated $A_{101}$ shows features assigned as $V_o$ that upon annealing for 10 min at 326 K result in what is described as subsurface oxygen vacancy clusters[16]—a phenomenon not observed in our work. This may be because heating could allow the $V_o$ to diffuse along thermally activated pathways into the subsurface and then bulk such that it is not possible to probe with STM. Previous STM studies have investigated the adsorption of $H_2O$,[18,20,22] $OH_t$,[18,22] CO,[22,37] and $O_2$[18,22,38] on $A_{101}$. The findings are unlike the bright features observed here with a number of tips.

As single atomic defects on $A_{101}$, the STM appearance of $OH_{br}$ assigned bright feature and $V_o$ are very similar (i.e., a bright feature above a sphere-like feature), making it difficult to differentiate the two species with STM alone. In the literature, low temperature STM shows that the adsorption of diatomic species on $A_{101}$, such as CO, $O_2$, and $OH_t$, presents "dimer-like" features where species are differentiated effectively by their behavior.[22] Similarly, $OH_{br}$ and $V_o$ can be differentiated by their behavior. In our STM, at room temperature, $OH_{br}$ has been shown to be stable on the surface, whereas $V_o$ stability on the surface is restricted to temperatures below 200 K.[16] Above 200 K, $V_o$ are increasingly mobile, resulting in subsurface vacancy cluster formation or $V_o$ migration to the bulk. The temperature dependent behavior of $OH_{br}$ and $V_o$ can be effectively used to differentiate the two species.

Previous STM studies of electron irradiated $A_{101}$ have been performed at 6−78 K, where $V_o$ are observed.[16−18] In these publications,[16−18] there is no report of $OH_{br}$ formation, which can be attributed to the low levels of residual $H_2O$ in the respective UHV chamber (base pressure at ×10$^{-11}$ to ×10$^{-12}$ mbar). Alternatively, an activation barrier to water dissociation may prevent $OH_{br}$ formation, as is the case on $R_{110}$.[39] At room temperature, STM[40] of electron irradiated $A_{101}$ has been pursued to understand Au and Pt nanoparticle interaction with $V_o$. Postelectron irradiation STM shows some features which are similar to the bright features shown in Figures 3−5, which were tentatively assigned to $V_o$. However, it has since become apparent that $V_o$ are unstable on the surface at room temperature.[16] Hence, it is reasonable to suppose that the previously observed features arise from $OH_{br}$ species, similar to the bright features observed in our work.

## 4. CONCLUSION

The formation of OH species on $A_{101}$ is a key step in $H_2O$ dissociation. We have electron irradiated $A_{101}$ to probe if the residual $H_2O$ in UHV is sufficient to quench the resulting $V_o$ and form $OH_{br}$ groups. Our STM images show that this results in the formation of bright features on the surface, which we assign as $OH_{br}$ species. This claim is supported by theoretical calculations[25,26] and our previously published spectroscopic measurements.[30]

## ■ AUTHOR INFORMATION

### Corresponding Author

*E-mail: g.thornton@ucl.ac.uk.

### ORCID

Geoff Thornton: 0000-0002-1616-5606

### Notes

The authors declare no competing financial interest.

## ■ ACKNOWLEDGMENTS

We thank Yu Zhang for useful discussions. This work was supported by the European Research Council Advanced Grant ENERGYSURF to G.T., EPSRC (EP/L015862/1), EU COST action 1104 and the Royal Society through a Wolfson Research Merit Award.

## REFERENCES

(1) Chen, X. B.; Shen, S. H.; Guo, L. J.; Mao, S. S. Semiconductor-Based Photocatalytic Hydrogen Generation. *Chem. Rev.* **2010**, *110*, 6503−6570.

(2) Fujishima, A.; Honda, K. Electrochemical Photolysis of Water at a Semiconductor Electroode. *Nature* **1972**, *238*, 37−38.

(3) Ni, M.; Leung, M. K. H.; Leung, D. Y. C.; Sumathy, K. A Review and Recent Developments in Photocatalytic Water-Splitting using $TiO_2$ for Hydrogen Production. *Renewable Sustainable Energy Rev.* **2007**, *11*, 401−425.

(4) Asahi, R.; Morikawa, T.; Irie, H.; Ohwaki, T. Nitrogen-Doped Titanium Dioxide as Visible-Light-Sensitive Photocatalyst: Designs, Developments, and Prospects. *Chem. Rev.* **2014**, *114*, 9824−9852.

(5) Hashimoto, K.; Irie, H.; Fujishima, A. $TiO_2$ Photocatalysis: A Historical Overview and Future Prospects. *Jpn. J. Appl. Phys. 1* **2005**, *44*, 8269−8285.

(6) Schneider, J.; Matsuoka, M.; Takeuchi, M.; Zhang, J. L.; Horiuchi, Y.; Anpo, M.; Bahnemann, D. W. Understanding $TiO_2$ Photocatalysis: Mechanisms and Materials. *Chem. Rev.* **2014**, *114*, 9919−9986.

(7) Zhang, H. J.; Chen, G. H.; Bahnemann, D. W. Photoelectrocatalytic Materials for Environmental Applications. *J. Mater. Chem.* **2009**, *19*, 5089−5121.

(8) Landmann, M.; Rauls, E.; Schmidt, W. G. The Electronic Structure and Optical Response of Rutile, Anatase and Brookite $TiO_2$. *J. Phys.: Condens. Matter* **2012**, *24*, 195503.

(9) Pang, C. L.; Lindsay, R.; Thornton, G. Chemical Reactions on Rutile $TiO_2$ (110). *Chem. Soc. Rev.* **2008**, *37*, 2328−2353.

(10) Pang, C. L.; Lindsay, R.; Thornton, G. Structure of Clean and Adsorbate-Covered Single-Crystal Rutile $TiO_2$ Surfaces. *Chem. Rev.* **2013**, *113*, 3887−3948.

(11) Diebold, U. The Surface Science of Titanium Dioxide. *Surf. Sci. Rep.* **2003**, *48*, 53−229.

(12) Thompson, T. L.; Yates, J. T. Surface Science Studies of the Photoactivation of $TiO_2$-New Photochemical Processes. *Chem. Rev.* **2006**, *106*, 4428−4453.

(13) Linsebigler, A. L.; Lu, G. Q.; Yates, J. T. Photocatalysis on $TiO_2$ Surfaces- Principles, Mechanism, and Selected Results. *Chem. Rev.* **1995**, *95*, 735−758.

(14) Hebenstreit, W.; Ruzycki, N.; Herman, G. S.; Gao, Y.; Diebold, U. Scanning Tunneling Microscopy Investigation of the $TiO_2$ Anatase (101) Surface. *Phys. Rev. B: Condens. Matter Mater. Phys.* **2000**, *62*, R16334−R16336.

(15) Treacy, J. P. W.; Hussain, H.; Torrelles, X.; Grinter, D. C.; Cabailh, G.; Bikondoa, O.; Nicklin, C.; Selcuk, S.; Selloni, A.; Lindsay, R.; et al. Geometric Structure of Anatase $TiO_2$ (101). *Phys. Rev. B: Condens. Matter Mater. Phys.* **2017**, *95*, 075416.

(16) Scheiber, P.; Fidler, M.; Dulub, O.; Schmid, M.; Diebold, U.; Hou, W. Y.; Aschauer, U.; Selloni, A. (Sub)Surface Mobility of Oxygen Vacancies at the $TiO_2$ Anatase (101) Surface. *Phys. Rev. Lett.* **2012**, *109*, 136103.

(17) Setvin, M.; Schmid, M.; Diebold, U. Aggregation and Electronically Induced Migration of Oxygen Vacancies in $TiO_2$ Anatase. *Phys. Rev. B: Condens. Matter Mater. Phys.* **2015**, *91*, 195403.

(18) Setvin, M.; Aschauer, U.; Hulva, J.; Simschitz, T.; Daniel, B.; Schmid, M.; Selloni, A.; Diebold, U. Following the Reduction of Oxygen on $TiO_2$ Anatase (101) Step by Step. *J. Am. Chem. Soc.* **2016**, *138*, 9565−9571.

(19) Herman, G. S.; Dohnalek, Z.; Ruzycki, N.; Diebold, U. Experimental Investigation of the Interaction of Water and Methanol with Anatase-$TiO_2$ (101). *J. Phys. Chem. B* **2003**, *107*, 2788−2795.

(20) He, Y. B.; Tilocca, A.; Dulub, O.; Selloni, A.; Diebold, U. Local Ordering and Electronic Signatures of Submonolayer Water on Anatase $TiO_2$ (101). *Nat. Mater.* **2009**, *8*, 585−589.

(21) Walle, L. E.; Borg, A.; Johansson, E. M. J.; Plogmaker, S.; Rensmo, H.; Uvdal, P.; Sandell, A. Mixed Dissociative and Molecular Water Adsorption on Anatase $TiO_2$ (101). *J. Phys. Chem. C* **2011**, *115*, 9545−9550.

(22) Setvin, M.; Daniel, B.; Aschauer, U.; Hou, W.; Li, Y. F.; Schmid, M.; Selloni, A.; Diebold, U. Identification of Adsorbed Molecules via STM Tip Manipulation: CO, $H_2O$, and $O_2$ on $TiO_2$ Anatase (101). *Phys. Chem. Chem. Phys.* **2014**, *16*, 21524−21530.

(23) Jackman, M. J.; Thomas, A. G.; Muryn, C. Photoelectron Spectroscopy Study of Stoichiometric and Reduced Anatase $TiO_2$ (101) Surfaces: The Effect of Subsurface Defects on Water Adsorption at Near-Ambient Pressures. *J. Phys. Chem. C* **2015**, *119*, 13682−13690.

(24) Geng, Z. H.; Chen, X.; Yang, W. S.; Guo, Q.; Xu, C. B.; Dai, D. X.; Yang, X. M. Highly Efficient Water Dissociation on Anatase $TiO_2$ (101). *J. Phys. Chem. C* **2016**, *120*, 26807−26813.

(25) Tilocca, A.; Selloni, A. Reaction Pathway and Free Energy Barrier for Defect-Induced Water Dissociation on the (101) Surface of $TiO_2$ Anatase. *J. Chem. Phys.* **2003**, *119*, 7445−7450.

(26) Tilocca, A.; Selloni, A. Structure and Reactivity of Water Layers on Defect-Free and Defective Anatase $TiO_2$ (101) Surfaces. *J. Phys. Chem. B* **2004**, *108*, 4743−4751.

(27) Selcuk, S.; Selloni, A. Facet-Dependent Trapping and Dynamics of Excess Electrons at Anatase $TiO_2$ Surfaces and Aqueous Interfaces. *Nat. Mater.* **2016**, *15*, 1107−1113.

(28) Futera, Z.; English, N. J. Exploring Rutile (110) and Anatase (101) $TiO_2$ Water Interfaces by Reactive Force-Field Simulations. *J. Phys. Chem. C* **2017**, *121*, 6701−6711.

(29) Stetsovych, O.; Todorovic, M.; Shimizu, T. K.; Moreno, C.; Ryan, J. W.; Leon, C. P.; Sagisaka, K.; Palomares, E.; Matolin, V.; Fujita, D.; et al. Atomic Species Identification at the (101) Anatase Surface by Simultaneous Scanning Tunnelling and Atomic Force Microscopy. *Nat. Commun.* **2015**, *6*, 7265.

(30) Payne, D. T.; Zhang, Y.; Pang, C. L.; Fielding, H. H.; Thornton, G. Creating Excess Electrons at the Anatase $TiO_2$ (101) Surface. *Top. Catal.* **2017**, *60*, 392−400.

(31) Setvin, M.; Daniel, B.; Mansfeldova, V.; Kavan, L.; Scheiber, P.; Fidler, M.; Schmid, M.; Diebold, U. Surface Preparation of $TiO_2$ Anatase (101): Pitfalls and How to Avoid Them. *Surf. Sci.* **2014**, *626*, 61−67.

(32) Setvin, M.; Franchini, C.; Hao, X. F.; Schmid, M.; Janotti, A.; Kaltak, M.; Van de Walle, C. G.; Kresse, G.; Diebold, U. Direct View at Excess Electrons in $TiO_2$ Rutile and Anatase. *Phys. Rev. Lett.* **2014**, *113*, 086402.

(33) Wendt, S.; Matthiesen, J.; Schaub, R.; Vestergaard, E. K.; Laegsgaard, E.; Besenbacher, F.; Hammer, B. Formation and Splitting of Paired Hydroxyl Groups on Reduced $TiO_2$ (110). *Phys. Rev. Lett.* **2006**, *96*, 066107.

(34) Zhang, Z.; Bondarchuk, O.; Kay, B. D.; White, J. M.; Dohnalek, Z. Imaging Water Dissociation on $TiO_2$ (110): Evidence for Inequivalent Geminate OH groups. *J. Phys. Chem. B* **2006**, *110*, 21840−21845.

(35) Pang, C. L.; Bikondoa, O.; Humphrey, D. S.; Papageorgiou, A. C.; Cabailh, G.; Ithnin, R.; Chen, Q.; Muryn, C. A.; Onishi, H.; Thornton, G. Tailored $TiO_2$ (110) Surfaces and their Reactivity. *Nanotechnology* **2006**, *17*, 5397−5405.

(36) Bikondoa, O.; Pang, C. L.; Ithnin, R.; Muryn, C. A.; Onishi, H.; Thornton, G. Direct Visualization of Defect-Mediated Dissociation of Water on $TiO_2$ (110). *Nat. Mater.* **2006**, *5*, 189−192.

(37) Setvin, M.; Buchholz, M.; Hou, W. Y.; Zhang, C.; Stoger, B.; Hulva, J.; Simschitz, T.; Shi, X.; Pavelec, J.; Parkinson, G. S.; et al. A Multitechnique Study of CO Adsorption on the $TiO_2$ Anatase (101) Surface. *J. Phys. Chem. C* **2015**, *119*, 21044−21052.

(38) Setvin, M.; Aschauer, U.; Scheiber, P.; Li, Y. F.; Hou, W. Y.; Schmid, M.; Selloni, A.; Diebold, U. Reaction of $O_2$ with Subsurface Oxygen Vacancies on $TiO_2$ Anatase (101). *Science* **2013**, *341*, 988−991.

(39) Brookes, I. M.; Muryn, C. A.; Thornton, G. Imaging Water Dissociation on $TiO_2$ (110). *Phys. Rev. Lett.* **2001**, *87*, 266103.

(40) Gong, X. Q.; Selloni, A.; Dulub, O.; Jacobson, P.; Diebold, U. Small Au and Pt Clusters at the Anatase $TiO_2$ (101) Surface: Behavior

at Terraces, Steps, and Surface Oxygen Vacancies. *J. Am. Chem. Soc.* **2008**, *130*, 370−381.

DOI: 10.1021/acs.jpcb.7b06955